I.M. BOLESTA,[1] M.M. VAKIV,[2] V.G. HAIDUCHOK,[2] I.I. KOLYCH,[1] A.A. KUSHNIR,[1] I.M. ROVETSKYY,[1] YU.M. FURGALA [1]

[1] Ivan Franko National University of Lviv, Faculty of Electronics and Computer Technologies, Chair of Radiophysics and Computer Technologies
  (107, Gen. Tarnavs'kyi Str., Lviv 79017, Ukraine; e-mail: Alex.Kuschnir@gmail.com)
[2] Scientific Production Enterprise "Karat"
  (202, Stryis'ka Str., Lviv 79031, Ukraine)

PACS 71.35.Cc, 71.45.Gm

PLASMON ABSORPTION BY SILVER NANOPARTICLES ON LiNbO₃ SURFACE

The morphology and optical spectra of silver nanoparticles sputtered onto lithium niobate substrates have been studied. Silver films with small mass thicknesses (from 0.5 to 3.0 nm) are found to form oblate spheroidal (disk-like) nanoparticles on the LiNbO₃ surface, with a radius of about 7 nm and a height of about 1.2 nm. The corresponding absorption spectra contain a band with a maximum at 520–640 nm, which is associated with the excitation of nanospheroid's plasmon mode. The location of the plasmon resonance maximum is found to depend on the sign of the lithium niobate surface charge, being equal to 564 nm for the positively charged surface and to 587 nm for the negatively charged one. A mechanism for the explanation of this dependence is proposed.

K e y w o r d s: surface plasmon resonance, atomic-force-microscopy morphology, silver nanoparticles, absorption spectra.

1. Introduction

The plasmon response of nanoparticles of noble metals located in the bulk or on the surface of dielectric matrices has been intensively studied in recent years. The optical response of metal nanoparticles, whose dimensions are much smaller than the light wavelength, is associated with the excitation of plasmon resonances. Localized surface plasmons, which are connected with oscillations of conduction electrons, play an important role in many domains of physics such as the amplification of light at its transmission through metal nanostructures [1, 2], application of materials with gold and silver nanoparticles in solar power engineering [3], development of biological

sensors [4, 5], creation of new materials [6], and so forth.

The existence of surface plasmons is "provided" by a negative value of the real part of the metal dielectric permittivity, $\mathrm{Re}\ \varepsilon_m < 0$. At the same time, surface plasmons are observed as resonances only at low dielectric losses. The latter are determined by the magnitude of the imaginary part of the metal dielectric permittivity; therefore, we have $\mathrm{Im}\ \varepsilon_m \ll |\mathrm{Re}\ \varepsilon_m|$ for plasmonic materials. The indicated conditions are well satisfied in such metals as Ag, Au, and Cu, which are considered as plasmonic materials.

Nano-sized metal particles, which are formed at the first stages of the sputtering of films, are interesting objects for the research of plasmon effects. It is so because, depending on technological parameters, it is possible to produce nanocomposites with various structures and metal phase contents. In particular, ultrathin metal films of silver with a struc-
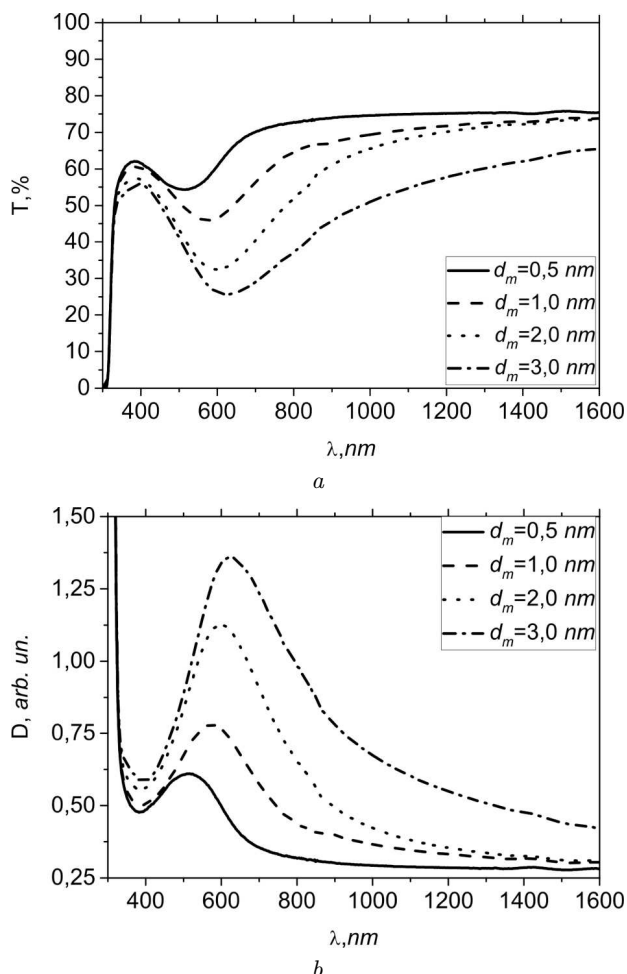
Fig. 1. Experimental transmission (*a*) and absorptions (*b*) spectra of silver films sputtered onto the positively charged LiNbO$_3$ surface to various mass thicknesses d_m

ture below the percolation threshold contain a conducting phase (metal nanoparticles) and a dielectric one (voids). They are considered as nano-sized metal-insulator composites with a fractal structure, in which there exist localized plasmons [7, 8].

In this work, the structure and the plasmon spectra of silver films with a structure below the percolation threshold, which were sputtered on single-crystalline lithium niobate (LiNbO$_3$) substrates, are studied.

2. Specimen Fabrication and Experimental Technique

Silver films were obtained, by using the method of magnetron sputtering in vacuum on an instal-

lation for combined sputtering COM-TH2-SP2-ION (TORR, USA). The films were sputtered onto $16 \times 8 \times 0.8$ mm^3-substrates. The latter were fabricated from single-crystalline lithium niobate, with the crystallographic axis Z being directed perpendicularly to the substrate plane. Since LiNbO$_3$ single crystals belong to the class of pyroelectrics, and the vector **P** is parallel to the axis Z, the substrate surfaces are characterized by different charge signs: positive and negative.

The film sputtering was performed at a rate of 0.7 Å/s. The substrate temperature was equal to 50 °C. The mass thickness of silver films was monitored with the help of a quartz generator [9] and varied within the limits from 0.5 to 3 nm.

The topology of the LiNbO$_3$ surface with sputtered films was researched with the use of an atomic force microscope (AFM) NT-MDT Solver Pro 47. It was registered in a semicontact regime, by applying an NSG10 probe with a tip radius of about 10 nm. Numerical parameters were obtained for separate elements of the structure of a film by segmenting the surface topology image, by using the watershed method [10] and determining whether that or another image segment corresponds to a particle. This procedure allowed us to distinguish the particle boundaries in the image, determine the particle shape, and find the geometrical parameters. In order to enhance the reliability of our results and to eliminate the influence of local inhomogeneities, the data obtained for the surface topology at various film sites were averaged over the ensemble.

The transmission and reflection spectra were measured in an interval of 300–1600 nm with a step of 1.0 nm on a double-beam spectrophotometer Shimadzu UV-3600 with a spectrometer slit bandwidth of 2.0 nm. A halogen lamp served as a light source. A photomultiplier was used as a detector in an interval of 300–960 nm, and an InGaAs photo diode played the role of a sensor in the wavelength interval above 960 nm. The reflection spectra were measured with the use of an ASR-3105 attachment with the complete specular reflection at an incidence angle of 5°.

3. Research Results and Their Discussion

The absorption spectra of Ag films sputtered onto a positively charged LiNbO$_3$ surface have a band, whose maximum shifts from 520 to 610 nm, as the mass thickness of the films grows (Fig. 1). This band

is associated with the surface plasmon resonance (SPR) in the silver nanoparticles that were formed on the LiNbO₃ surface at the initial stages of metal sputtering. The long-wave shift of the band maximum with the growth of the mass film thickness is related to the size increase of silver nanoparticles. The asymmetric character of absorption spectra is connected with the influence of the substrate on the absorption spectrum in the short-wave section [11] and with the metal absorption growth in the long-wave interval at larger mass thicknesses of the films [12].

The frequency spectrum of surface oscillation modes for a spherical particle is given by the expression [13]

$$\omega_l = \frac{\omega_p}{\sqrt{1 + \frac{l+1}{l}\varepsilon_m}}, \qquad (1)$$

where $\omega_p = \sqrt{\frac{4\pi n e^2}{m_e}}$ is the plasma frequency of free electrons; n, e, and m_e are the concentration, charge, and mass, respectively, of conduction electrons; ε_m is the complex dielectric permittivity of the medium; and $l = 1, 2, 3, ...$ specifies the oscillation multipole number. In particular, dipole oscillations ($l = 1$) prevail in particles with small dimensions, whereas quadrupole ($l = 2$) oscillation modes manifest themselves in particles with larger dimensions ($r > 50$ nm). The frequency of dipole oscillations can be determined from the Fröhlich condition Re $\varepsilon = 2\varepsilon_m$.

In Fig. 2, the SPR spectra of the silver nanoparticles obtained by sputtering Ag in the same working cycle on a glass substrate and on positively and negatively charged LiNbO₃ surfaces are shown. One can see that the spectral location of the SPR band for the silver nanoparticles on the LiNbO₃ surface (564 nm for the positively charged surface and 587 nm for the negatively charged one) is substantially shifted toward the long-wave region in comparison with the maximum in the spectrum of Ag nanoparticles on the glass substrate (532 nm). The mass thicknesses of Ag films sputtered onto the LiNbO₃ and glass surfaces in the same working cycle are identical. Therefore, the difference between the maximum positions can be a result of a number of factors. The main of them is associated with different shapes of particles that were formed on the glass and LiNbO₃ surfaces.

In Fig. 3, *a*, the AFM topology of the surface of the Ag film sputtered on the LiNbO₃ substrate is
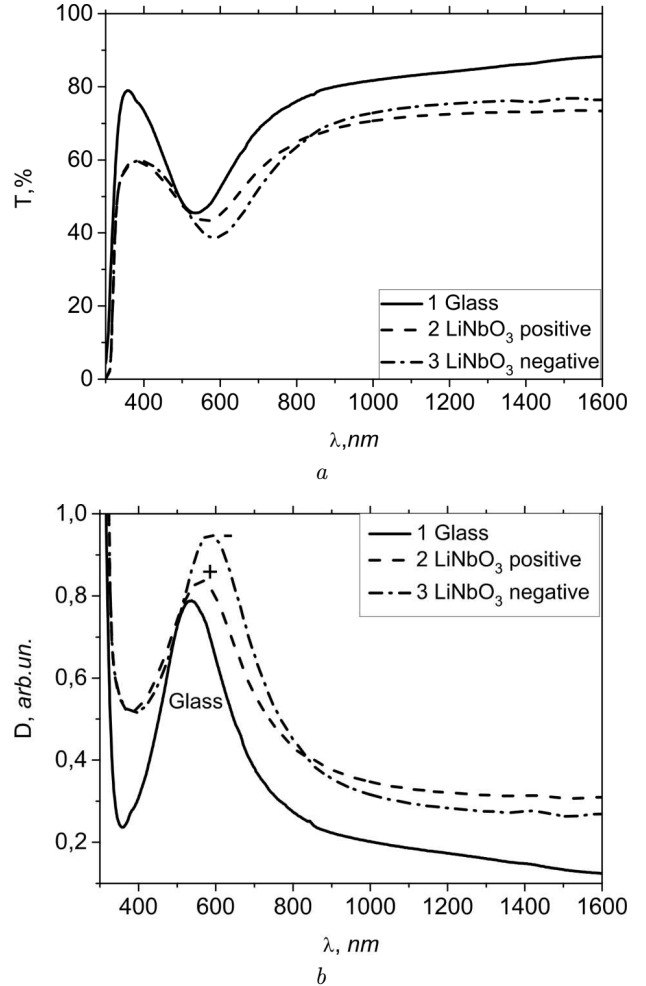
Fig. 2. Transmission (*a*) and absorption (*b*) spectra of silver films 1 nm in mass thickness on the glass substrate (*1*) and the positively (*2*) and negatively (*3*) charged LiNbO₃ surfaces

depicted. The watershed method [10] was applied to distinguish the boundaries of nanoparticles, which allowed us to determine the distributions of nanoparticles over their equivalent radii, heights, and distances to the nearest neighbor (Fig. 4). From the analysis of the data obtained, it follows that the sputtering of an Ag film to the mass thickness $d_m = 1$ nm on the LiNbO₃ surface gives rise to the formation of particles in the form of oblate spheroids (disks) with an average radius of about 7 nm and a height of about 1.2 nm. The r/h-ratio for the particles can be calculated as the ratio between the principal axes of an oblate spheroid, $a/c \approx 5.8$.
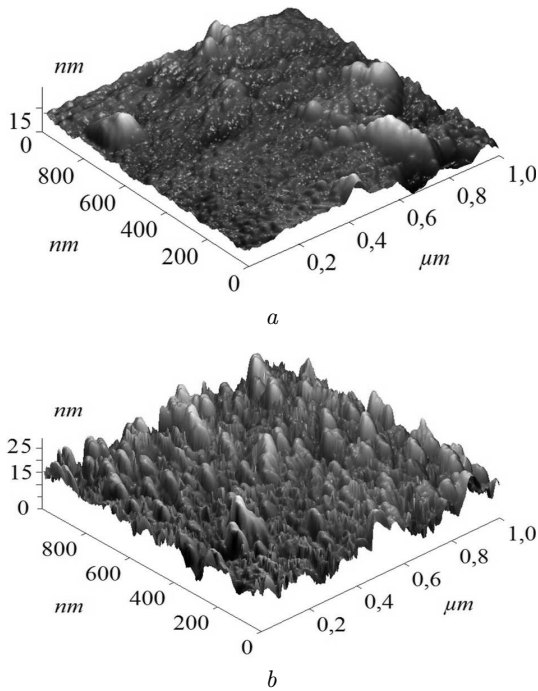
Fig. 3. AFM images of the surface morphology of an Ag film 1 nm in mass thickness sputtered onto the positively charged LiNbO$_3$ (*a*) and glass (*b*) surfaces

In view of the AFM data, we may assume that spheroidal silver nanoparticles are formed on the LiNbO$_3$ surface in the course of metal sputtering. Such particles are characterized by longitudinal and transverse modes of charge oscillations [15]. The mode associated with the longitudinal (along the *a*-axis) oscillations of charge carriers is shifted toward the long-wave spectral region with respect to the same mode in a spherical particle. Therefore, the long-wave band shift of SPR in Ag nanoparticles on the LiNbO$_3$ substrate in comparison with that in the case of a glass substrate can be explained as the manifestation of only the longitudinal mode of oscillations in disk-shaped silver nanoparticles in the LiNbO$_3$–Ag spectrum.

In order to verify this hypothesis, we calculated the relevant spectra in the quasistatic approximation and making no allowance for the interaction between the particles. The substantiation of this calculation method is based on the fact that the distance between the particles (Fig. 4, *c*) exceeds their dimensions. Since the LiNbO$_3$–Ag structure contains nanoparticles with various radii and heights (Fig. 4),
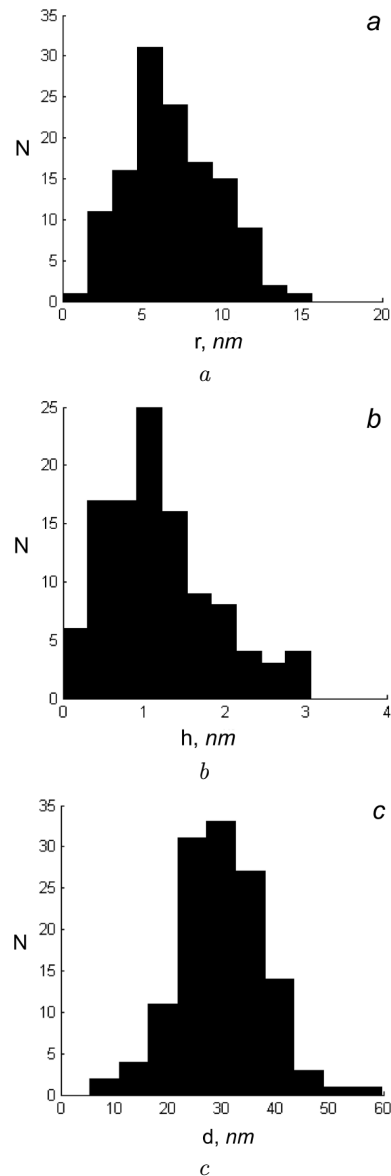
Fig. 4. Distributions of silver nanoparticles over their radii (*a*), heights (*b*), and distances between them (*c*), which were determined from the AFM images for the silver film with $d_m = 1.0$ nm sputtered onto the positively charged LiNbO$_3$ surface

the calculated spectrum is a sum of spectra of spheroidal nanoparticles with different a/c-ratios.

In order to implement the proposed method, a forecasted set of n different ratios $a/c = k$ was selected. In our calculations, the value of k was changed from 1 to 20 with a step of 1, i.e. $n = 20$. The ex-

42

tinction spectra were calculated for all particles with the chosen a/c-ratios. The calculations were carried out – in the electrostatic approximation and in the wavelength interval, where experimental spectra were measured – using the formula [15, 16]

$$C = 4\pi k \mathrm{Im}\left(\alpha_x \frac{2}{3} + \alpha_z \frac{1}{3}\right) + \frac{8\pi}{3}k^4\left(|\alpha_x|^2\frac{2}{3} + |\alpha_z|^2\frac{1}{3}\right),$$

(2)

where α_x and α_z are the spheroid polarizabilities corresponding to the oscillation modes along the axes a and c, respectively. In formula (2), it was taken into account that, in the case of equal axes ($a = b$), the corresponding polarizabilities are also identical ($\alpha_x = \alpha_y$). The values of polarizabilities are given by the relations [15, 16]

$$\alpha_x = \frac{ca^2}{3}\frac{\varepsilon(\omega) - \varepsilon_m}{\varepsilon_m + L_1(\varepsilon(\omega) - \varepsilon_m)},$$

(3)

$$\alpha_z = \frac{ca^2}{3}\frac{\varepsilon(\omega) - \varepsilon_m}{\varepsilon_m + L_0(\varepsilon(\omega) - \varepsilon_m)},$$

(4)

where ε_m is the dielectric permittivity of the medium, and $\varepsilon(\omega)$ the dielectric permittivity of a metal particle. The expressions for α_x and α_z also include the principal depolarization coefficients L_1 and L_0. The forms of general expressions for them depend on the spheroid shape [15, 16]:

$$L_0 = \left(1 + \xi_0^2\right)\left(1 - \xi_0 \, \mathrm{arcctg}\, \xi_0\right), \quad L_1 = \frac{1}{2}(1 - L_0),$$

(5)

where $\xi_0 = \sqrt{\frac{c^2}{a^2 - c^2}}$ is the geometrical factor.

In the "wavelength space", the experimental spectrum E_l can be presented by a vector containing m "components" for various wavelengths λ_i ($i = 1, \dots, m$). In this "space", the calculated C_{ji}-spectra ($j = 1, ..., n$; $i = 1, \dots, m$) form a matrix **C** with n columns and m rows. Each matrix element C_{ji} corresponds to the extinction of a nanoparticle with the coefficient k_i at the wavelength λ_j. In the framework of this representation, every point E_l on the experimental curve can be approximated by a linear combination of the extinction values C_{jl} ($j = 1, ..., n$) calculated for the chosen wavelength λ_l:

$$E_l = \sum_{j=1}^{n} C_{jl}\omega_j,$$

(6)

where ω_j is the weight of the contribution made by the j-th particle to the total spectrum. Then the approximation of the experimental spectrum E is reached by minimizing the mean-square deviation

$$S = \sum_{i=1}^{m}\left(E_i - \sum_{j=1}^{n} C_{ji}\omega_j\right)^2.$$

(7)

The minimization procedure can be performed in two ways: using the gradient descent method or the Monte Carlo one. The approximation accuracy was determined from the root-mean-square deviation (RMSD), by using the formula

$$\delta = \frac{\sqrt{S}}{\sum_{i=1}^{m}|E_i|}.$$

(8)

To solve Eq. (8), the initial values of the vector W should be given – for example, $W = W_0 = 1$ – for which the spectrum and the RMSD between the experimental and theoretical curves are calculated.

The first step of the cycle consists in changing all weight coefficients by a random value within the interval $(0, 2w_i]$. In other words, each weight can either double its value or tend to zero. After the new curve has been built, a new RMSD is calculated. In the considered method, the RMSD value plays the role of energy in the classical Monte Carlo method [17]. Therefore, if the RMSD for the new weight set diminishes, the latter is accepted. Otherwise, i.e. when the RMSD increases, the changed weight set is rejected. This procedure does not result in the sticking to a local solution, because the weights can considerably change at their random correction.

Figure 5, *a* illustrates the experimental spectra (solid curves) and their fitting approximations, which allowed the distributions of nanoparticles over the ratio a/c to be determined. As one can see, the distribution obtained from the AFM data is slightly shifted toward the region of larger k with respect to the data calculated, by using the proposed method. This effect was already explained by us earlier [12]. It arises owing to an imperfection of atomic force microscopy, namely, because of a finite size of the scanning element, the AFM probe. This effect is especially pronounced for objects, whose dimensions are comparable with the curvature radius of an AFM probe (about 10 nm).

a

b
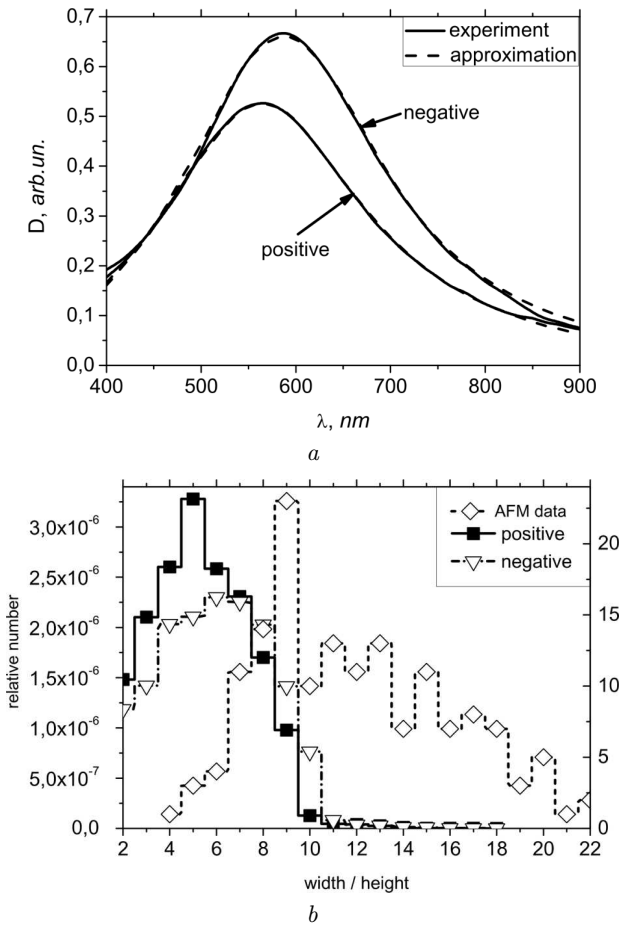
Fig. 5. Extinction spectra of silver films on the LiNbO$_3$ surface and their approximations (*a*). Distributions of silver nanoparticles over the ratio between their principal axes, which were obtained from morphological and optical researches (*b*)

We also found that the spectral position of the plasmon resonance band in Ag nanoparticles on the LiNbO$_3$ surface depends on the sign of surface charge: the band maximum is located at 587 nm for the negative charge and at 564 nm for the positive one (Fig. 2). Let us analyze a probable origin of this spectral shift by $\Delta\lambda = 23$ nm. In the framework of Mie theory, such a location change can be induced only by a variation in the free carrier concentration [18], because the results of AFM researches testify that the surface topology is identical in both cases. Since the plasmon resonance wavelength $\lambda_{\max} \sim 1/\sqrt{n}$ [13], the long-wave shift observed in the case of positively charged surface is a result of the "exclusion" of a certain fraction of free charge carriers from the oscilla-
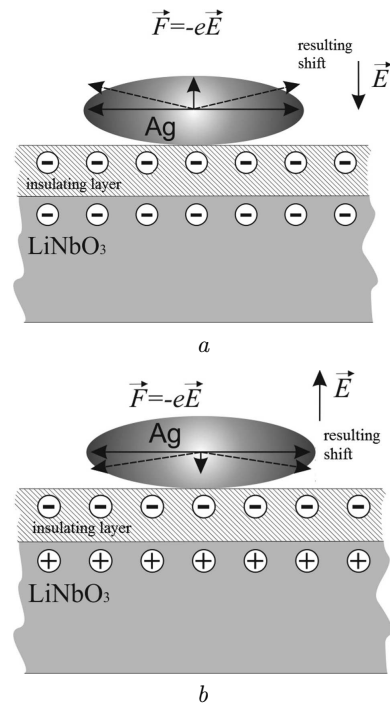
Fig. 6. Schematic diagrams illustrating a possible mechanism that gives rise to a shift of the maximum in the plasmon absorption band in the cases of negatively (*a*) and positively (*b*) charged LiNbO$_3$ surfaces

tion motion, through which the surface plasmon resonance is realized. We evaluated that, for the shift to equal $\Delta\lambda = 23$ nm, the concentration n_- should decrease to $n_- = 0.93n_+$.

Let us analyze a probable mechanism of how the surface charge can affect the concentration change of free charge carriers participating in the surface plasmon resonance. The electric field created by negative charges pushes free charge carriers to the nanoparticle surface. The magnitude of corresponding force can be enhanced owing to the presence of built-in negative charges in the dielectric layer that exists between the LiNbO$_3$ surface and silver. As a result, the free charge carriers in the nanoparticle, in addition to the field of a light wave, are subjected to the action of the dc field, the strength of which can be considerable due to the nano-sized values of height h. Therefore, the resulting shift occurs at a certain angle with respect to the spheroid a-axis, which is equivalent to a reduction in the number of charge carriers contributing to the longitudinal plasmon mode of a nanospheroid.

In the case where silver nanoparticles are deposited on the positively charged LiNbO$_3$ surface, the field E_+ becomes partially or completely compensated by the field of the built-in charge $(-)$. Therefore, the deviation of plasmon oscillations from the axis is either lower or absent altogether.

4. Conclusions

To summarize, the obtained results of our research concerning the optical spectra and the structure of silver films on the lithium niobate surface allow the following conclusions to be drawn. The evolution of absorption spectra for the examined films is similar to that for films on the glass surface. The method proposed by us for evaluating the parameters of a film structure on the basis of optical data gives a good agreement with the experiment, which makes it suitable for practical applications. The revealed difference between the positions of the maximum in the absorption spectra of silver films on the lithium niobate surface with different signs of surface charge can be explained by the influence of the charge field on the motion of free electrons in the metal nanoparticles.

1. Sh. Zou, G.C. Schatz. Silver nanoparticle array structures that produce giant enhancements in electromagnetic fields. *Chem. Phys. Lett.* **403**, 62 (2005) [DOI: 10.1016/j.cplett.2004.12.107].
2. I. Bolesta. Surface plasmon-polaritons. *Elektron. Inform. Tekhnol.* **2**, 3 (2012).
3. R.M. Navarro Yerga, M.C. Álvarez Galván, F. del Valle, J.A. Villoria de la Mano, J.L.G. Fierro. Water splitting on semiconductor catalysts under visible-light irradiation. *Chem. Sus. Chem.* **2**, 471 (2009) [DOI: 10.1002/cssc.200900018].
4. M. Hu, J. Chen, Z.Y. Li, L. Au, G.V. Hartland, X. Li, M. Marquez, Y. Xia. Gold nanostructures: engineering their plasmonic properties for biomedical applications. *Chem. Soc. Rev.* **35**, 1084 (2006) [DOI: 10.1039/B517615H].
5. M.A. Garcia. *Surface Plasmons in Biomedicine Recent Developments in Bio-Nanocomposites for Biomedical Applications* (Nova Science, 2011).
6. M.A. Garcia. Surface plasmons in metallic nanoparticles: fundamentals and applications. *J. Phys. D* **44**, 283001 (2011) [DOI: 10.1088/0022-3727/44/28/283001].
7. S.V. Karpov, V.S. Gerasimov, I.L. Isaev, V.A. Markel. Local anisotropy and giant enhancement of local electromagnetic fields in fractal aggregates of metal nanoparticles. *Phys. Rev. B* **72**, 205425 (2005) [DOI: 10.1103/PhysRevB.72.205425].
8. I. Bolesta, O. Kushnir, B. Kulyk, V. Gavrylyukh. Fractal structure of ultra-thin silver films. *Visn. Lviv. Univ. Ser. Fiz.* **47**, 130 (2012).
9. L.B. Katsnelson, Sh.A. Furman. Method for measuring the thickness of thin films during their fabrication. *Author's certificate 216961 USSR* (published April 26, 1968) (in Russian).
10. L. Shafarenko, M. Petrou, J. Kittler. Automatic watershed segmentation of randomly textured color images. *IEEE Trans. Image Process.* **6**, 1530 (1997) [DOI: 10.1109/83.641413].
11. M. Cesaria, A.P. Caricato, M. Martino. Realistic absorption coefficient of ultrathin films. *J. Opt.* **14**, 105701 (2012).
12. I.M. Bolesta, A.V. Borodchuk, A.A. Kushnir, I.I. Kolych, I.I. Syworotka. Morphology and absorption spectra of ultra-thin films of silver. *J. Phys. Stud.* **15**, 4703 (2011).
13. M. Born, E. Wolf. *Principles of Optics* (Cambridge Univ. Press, 2000).
14. I.M. Bolesta, O.O. Kushnir. AFM microscopy and optical studies for the shape of particles in ultrathin silver films. *Ukr. J. Phys. Opt.* **13**, 165 (2012) [DOI: 10.3116/16091833/13/3/165/2012].
15. V.V. Klimov. *Nanoplasmonics* (Fizmatlit, 2010) (in Russian).
16. S.A. Maier. *Plasmonics: Fundamentals and Applications* (Springer, 2007).
17. N. Metropolis, S. Ulam. The Monte Carlo method. *J. Am. Stat. Assoc.* **44**, 335 (1949) [DOI: 10.1080/01621459.1949.10483310].
18. G. Mie. Beiträge zur Optik trüber Medien, speziell kolloidaler Metallösungen. *Ann. Phys.* **330**, 377 (1908) [DOI: 10.1002/andp.19083300302].

І.М. Болеста, М.М. Ваків, В.Г. Гайдучок,
І.І. Колич, О.О. Кушнір, І.М. Ровецький, Ю.М. Фургала

ПЛАЗМОННЕ ПОГЛИНАННЯ
НАНОЧАСТИНОК СРІБЛА НА ПОВЕРХНІ LiNbO$_3$

Р е з ю м е

Досліджено морфологію та оптичні спектри наночастинок срібла, напилених на підкладки ніобату літію. Встановлено, що в області масових товщин (від 0,5 до 3 нм) на поверхні LiNbO$_3$ плівки срібла формують наночастинки у формі сплюснутих сфероїдів (дисків) з радіусом $\sim$7 нм і висотою $\sim$1,2 нм. У спектрах поглинання спостерігається смуга з максимумом в області 520–640 нм, яка пов'язується зі збудженням плазмонної моди наносфероїда. Встановлено, що максимум смуги плазмонного резонансу залежить від знака заряду поверхні ніобату літію та дорівнює 564 нм для позитивно та 587 нм для негативно заряджених поверхонь. Запропоновано механізм залежності положення максимуму ППР від знака заряду поверхні.